Polymer Entrapment Flash Pyrolysis for the Preparation of Nanoscale Iridium-Free Oxygen Evolution Electrocatalysts

Pei-Chieh Shih,[a] Cheng Zhang,[a] Harshit Raheja,[a] Cheng-Jun Sun[b] and Hong Yang*[a]

Abstract: This paper describes the use of a new polymer entrapment flash pyrolysis (PEFP) method for making nanoscale yttrium ruthenate (Y2Ru2O$_{7-\delta}$) electrocatalysts. This approach effectively reduced the synthesis temperature of phase-pure pyrochlore catalysts from 1000 °C to 550 °C, and greatly suppressed the sintering of catalyst particles. The supported nanocrystalline $Y_2Ru_2O_{7-\delta}$ catalysts showed enhanced activity towards oxygen evolution reaction (OER) in acidic electrolyte and were stable at 1.50 V for the comparative study (> 20 h) under the current density of 10 mA/cm$^2_{geo}$ in chronopotentiometry testing. This is equivalent to an overpotential value of 270 mV, about half of that for the reference IrO_2 catalyst. X-ray absorption spectroscopy (XAS) and transmission electron microscopy (TEM) analysis showed the high surface area $Y_2Ru_2O_{7-\delta}$ catalyst had an oxygen deficient structure. This study provides a route to the synthesis of fine ceramic (or oxide)-based electrocatalysts for making high performing electrocatalysts.

Introduction

Highly active and stable oxygen evolution reaction (OER) catalysts are needed to advance the technology of energy conversion and storage, such as electrolysis devices for direct water splitting[1-21] and metal-air batteries.[22] Development of active and stable OER catalysts however is challenging due to the intrinsically sluggish OER kinetic and instability under the harsh acidic environment, under which low-temperature polymer electrolyte membrane (PEM)-based electrolysis devices operate.[23, 24] Iridium oxide (IrO_2) has often been used as the catalyst in the PEM-based electrolyzer under acidic conditions.[24-26] However, the OER activity of IrO_2 is far from ideal not only because of its low activity, but also an exceptionally low earth abundance of Ir element, which posts another hurdle for large scale applications. Thus, development of alternative catalysts with improved OER activity and stability is highly desirable for the deployment of water electrolysis devices at scale.

Recently, single- and multiple-phase solids with the perovskite (ABO_3) and pyrochlore ($A_2B_2O_7$) structures have been discovered as new classes of OER catalysts. $Pb_2Ru_2O_{6.5}$,[27] Ba_2MIrO_6,[28] $Bi_2Ir_2O_7$,[29, 30] $IrO_x/SrIrO_3$,[31] $Y_2Ru_2O_{7-\delta}$,[8] $Y_2Ir_2O_7$,[10] $IrO_x/Y_2Ir_2O_7$,[32] $Y_2[Ru_{1.6}Y_{0.4}]O_{7-\delta}$,[9] and 6H-$SrIrO_3$,[33] are among such catalysts showing high OER activity.[34-37] Besides the emphasis on the electronic structures of the metal ions, oxygen defect is also attributed to the enhanced OER activities. Among them, Ir-based catalysts (e.g., $IrO_x/SrIrO_3$, 6H-$SrIrO_3$ and $Y_2Ir_2O_7$) have been reported to exhibit good stability at 10 mA/cm^2 under acidic conditions.[10, 31, 33]

For the OER performance, electrical conductivity is an important factor to consider in optimizing the activity and stability of these electrocatalysts because metal oxides are often electrically insulating. While enhancing the conductivity by using dopants may help, the level of dopant used is typically low and the effect is still limited.[38, 39] An alternative is to use conductive supports and operate under low overpotential conditions to improve the efficiency of current collections. In the latter approach, the size control of these catalysts could be important, because nanometer (nm)-sized particles with large surface areas are often necessary to make nanocomposites with good conductivity. For those recently developed pyrochlore-type catalysts, this requirement posts a synthetic challenge because perovskite- and pyrochlore-type solids usually require heating processes at high temperatures (> 900 °C), which could cause extensive sintering of nanoparticles.

Here we present a synthetic strategy based on the polymer entrapment flash pyrolysis (PEFP) method to make nanoscale pyrochlore $Y_2Ru_2O_{7-\delta}$ electrocatalysts. In this approach polyvinyl alcohol (PVA) is used as the long-chain polymer to form a charged organic network for the confinement of ions species. Polymer entrapment (PE) is a newly developed approach to the synthesis of electrode active materials such as $LiMnO_2$ and $LiFePO_4$ for Li-ion batteries.[40, 41] In this method, long-chain polymers could spatially confine metal ion precursors in organic network to limit the diffusion of metal ions and thus favor the formation of nanoscale oxides. We further developed the flash pyrolysis to facilitate the formation of the right phase with mixed metal ion precursors at a low temperature. Experimentally, we discovered that formation of phase pure pyrochlore-type nanoparticles could even be made at 550 °C using the PEFP method. This as-made $Y_2Ru_2O_{7-\delta}$ catalyst (PEFP-550) was characterized and compared with those made from sol-gel precursors at 1000 °C (solgel-1000).[8] X-ray diffractometer (XRD), energy-dispersive X-ray spectroscopy (EDS), X-ray absorption near-edge structure (XANES) spectra and extended X-ray absorption fine structure (EXAFS) spectra analysis show the formation of phase pure pyrochlore $Y_2Ru_2O_{7-\delta}$ catalysts. Scanning electron microscopy (SEM) and transmission electron microscopy (TEM) analysis indicate the PEFP-550 catalyst has higher specific surface area with smaller crystalline size than those made by the sol-gel method. This $Y_2Ru_2O_{7-\delta}$ OER catalyst (PEFP-550) exhibited an ultralow overpotential of 270 mV at a constant current density of 10 mA/cm^2 in a 0.1 M $HClO_4$ electrolyte solution (*vs*. 590 mV for IrO_2, > 20 h).

[a] Dr. P.-C. Shih, C. Zhang, H. Raheja, Prof. H. Yang
Department of Chemical and Biomolecular Engineering
University of Illinois at Urbana-Champaign
600 South Mathews Avenue, Urbana, Illinois 61801, United States
E-mail: hy66@illinois.edu

[b] Dr. C.-J. Sun
X-ray Science Division
Argonne National Laboratory
9700 South Cass Avenue, Argonne, Illinois 60439, United States

Supporting information for this article is given via a link at the end of the document.

Results and Discussion

Synthesis of nanoscale yttrium ruthenate electrocatalyst

Phase pure $Y_2Ru_2O_{7-\delta}$ nanocrystalline was prepared by PEFP method using PVA (Mw = 9,000 - 10,000) as the entrapment polymer (**Scheme 1**). A solution of 20 wt% PVA in DI water was prepared prior to the synthesis to ensure uniform mixing of metal precursors in PVA matrices. The amount of PVA solution added was based on the balanced charges. A cation/anion ratio of 1:12, which corresponds to a $Y(NO_3)_3$:$Ru(NO)(NO_3)_x(OH)_y$:PVA (monomer) molar ratio of 1:1:84, was used to prepare the phase pure $Y_2Ru_2O_{7-\delta}$ nanoparticles. After drying, the obtained solid was treated in two steps. First, it was heated on a hot plate with surface temperature set at 300 ºC to form an ionic network. The formed dark grey material was collected and underwent a second step of flash pyrolysis at 550 ºC to form the $Y_2Ru_2O_{7-\delta}$ pyrochlore nanocrystalline.

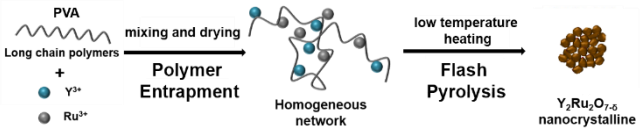

Scheme 1. Illustration of the PEFP method for making the $Y_2Ru_2O_{7-\delta}$ nanocrystalline OER catalysts.

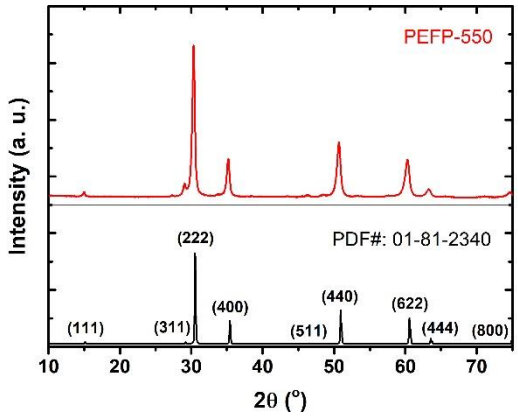

Figure 1. Powder XRD patterns of the $Y_2Ru_2O_{7-\delta}$ catalyst synthesized by the PEFP method at 550 °C (PEFP-550).

Figure 1 shows the XRD pattern of the powder product (PEFP-550) synthesized at 550 ºC by the PEFP method. All diffraction peaks can be assigned to the cubic phase pyrochlore of $Y_2Ru_2O_{7-\delta}$ in Fd-3m symmetry (PDF#: 01-81-2340). The Y:Ru ratio of this $Y_2Ru_2O_{7-\delta}$ product was about 1:1 as examined by the EDS analysis (**Figure S1**). Unlike $Y_2[Ru_{1.6}Y_{0.4}]O_{7-\delta}$ OER catalysts,[9] no mixed B-site ions were observed in this pyrochlore product ($A_2B_2O_{7-\delta}$).

Figure 2a shows the representative and magnified (inset) SEM images of the PEFP-550 catalyst. The primary particle size was measured to be around 40 ± 10 nm with no extensive sintering across the sample. The high-resolution TEM image shows individual grains are highly crystalline (**Figure 2b**). The d-spacing of the lattice was determined to be 2.99 Å. This value agrees with the lattice spacing of 2.94 Å for a typical $Y_2Ru_2O_7$ pyrochlore solid, corresponding to the (222) plane.

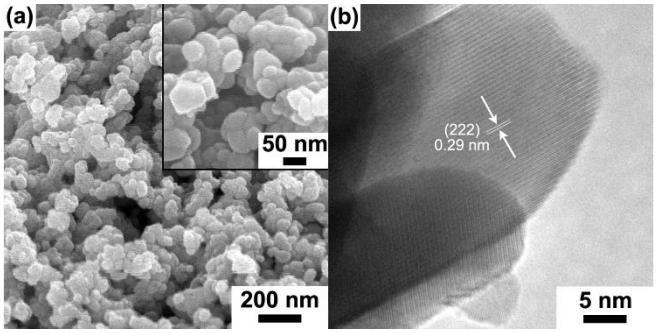

Figure 2. (a) SEM image and (b) TEM micrograph of the $Y_2Ru_2O_{7-\delta}$ catalyst synthesized at 550 °C (PEFP-550). Inset in (a) is a magnified image showing the grain size of particles.

Figure 3 shows the nitrogen isotherm and Brunnauer-Emmett-Teller (BET) surface area analysis for this catalyst. The specific surface area was determined to be 14.8 m^2/g, which was more than double of that of the $Y_2Ru_2O_{7-\delta}$ OER catalyst synthesized by the sol-gel method (7.2 m^2/g). The result agrees with the SEM observation, in which the average size (~40 nm) of nanoparticles was smaller than those $Y_2Ru_2O_{7-\delta}$ catalysts made by sol-gel synthesis (average size of > 100 nm).[8]

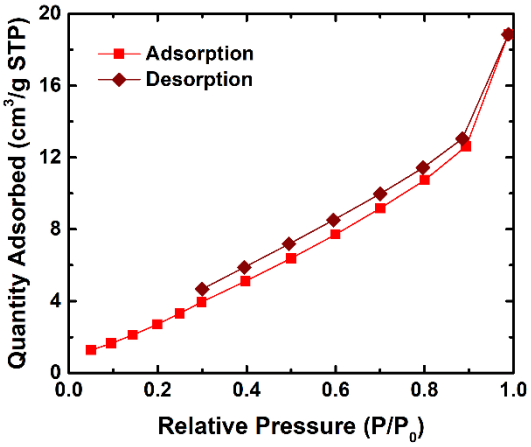

Figure 3. Nitrogen isotherm of the PEFP-550 OER catalyst. BET surface area was calculated from the adsorption curve for $P/P_0 < 0.4$.

Unlike those binary oxides (IrO_2, RuO_2, and Y_2O_3), phase purity and size of ternary oxides are very sensitive to the synthesis conditions and reaction mixtures. We thus examined the effects of several key synthetic parameters on the formation of phase-pure pyrochlore $Y_2Ru_2O_{7-\delta}$ nanoparticle catalysts. **Figure 4a** shows the XRD patterns of solid products obtained at the reaction temperature of 500 ºC for 6 h using a reaction mixture with the metal ions to PVA ratio at either 6:1 or 1:6. In either case, the resulting solid was found to be made of mainly tetragonal phase RuO_2 (PDF#: 00-40-1290) and amorphous solids. This result indicates that an optimal polymer to cation ratio is necessary to confine metal ion precursors uniformly for making $Y_2Ru_2O_{7-\delta}$ nanoparticles. SEM images further show that the solid products made at metal-ions to PVA ratios of 6:1 and 1:6 had a broad size distribution (**Figure S2**).

Figure 4b shows the XRD patterns of the solid products made at different temperatures using the precursor mixture at the

metal-ions to PVA ratio of 1:12, the same as the one for making the PEFP-550 catalyst. The solid formed however was amorphous without any high crystalline product if the reaction temperature was 200 ºC. Tetragonal phase RuO_2 was formed, together with the amorphous materials when the temperature increased to 500 ºC. This result indicates that the optimal reaction mixture should have a metal-ion to PVA ratio of 1:12 ratio in order to have enough polymers to uniformly disperse the metal ions in precursors, though only binary oxide of RuO_2 could form if the reaction temperature was 500 ºC and lower. In another word, 500 ºC is not sufficiently high for making ternary oxide of $Y_2Ru_2O_{7-\delta}$ pyrochlore. SEM images show that powders made at 200 ºC and 500 ºC had irregular shapes and sizes, indicating they were likely made of mixtures (**Figure S3**).

The ramping rate also affected the formation of phase pure $Y_2Ru_2O_{7-\delta}$ at low temperature. **Figure 4c** shows the XRD pattern of $Y_2Ru_2O_{7-\delta}$ made by PEFP synthesis at 550 ºC at a ramping rate of 5 ºC/min. While the $Y_2Ru_2O_{7-\delta}$ pyrochlore phase was formed, the by-products of RuO_2 and Y_2O_3 were also produced.

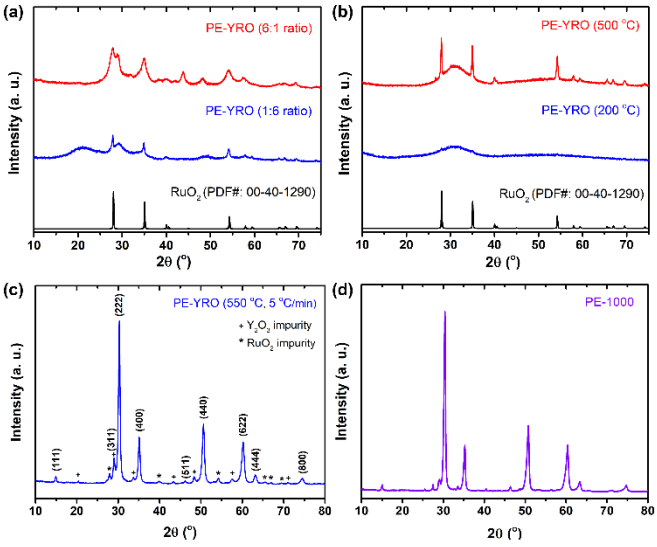

Fig. 4 Powder XRD patterns of the products synthesized using the PE method (PE-YRO) at different (a) metal ion to polymer ratios, (b) temperatures, and following (c and d) different procedures. The sample PE-550 shown in (c) was made at 550 °C with a ramping rate of 5 °C/min, and the PE-1000 in (d) was made at 1000 °C. Symbols of "+" and "*" in (c) indicate the diffractions from Y_2O_3 and RuO_2, respectively.

The formation of RuO_2 and Y_2O_3 upon the heating process at relatively low temperature is feasible because these binary oxide phases have a lower formation temperature than pyrochlore phase.[25, 42, 43] Flash pyrolysis thus is necessary to facilitate the various ions to react within confined environments in a short time and at low temperatures. This data demonstrates experimentally using PEFP is critical for making the pure phase of $Y_2Ru_2O_{7-\delta}$ pyrochlore. **Figure S4** shows the SEM image of sample made at 550 ºC at a rate of 5 ºC/min. The product had a primary particle size of 10 - 50 nm, which is comparable to the PEFP-550 catalyst using the flash pyrolysis approach. This observation indicates that heating rate did not have dramatic effect on the particle size made by this confinement method. The particle size was closely related to crystalline phase, which the reaction temperature is a major factor.

We tested the effects of synthesis temperature on the structure of the products. **Figure 4d** shows the XRD pattern of the $Y_2Ru_2O_{7-\delta}$ catalyst made by polymer entrapment at 1000 ºC (PE-1000). Compared with the $Y_2Ru_2O_{7-\delta}$ catalyst made by sol-gel synthesis at 1000 ºC (**Figure S5**), both samples were phase pure $Y_2Ru_2O_{7-\delta}$, although the PE-1000 catalyst had broader peaks and smaller grain size than the one made by the sol-gel method (**Figure S6)**. Particle sintering was observed for the catalyst made at 1000 ºC, even by the polymer entrapment method (PE-1000), resulting in the growth in primary particle size to 100 - 200 nm in diameter. The result indicates that PEFP synthesis is favored for making small particles with even those phases typically formed at much higher temperature, such as $Y_2Ru_2O_{7-\delta}$ pyrochlore. Even for the PE-1000 catalyst, within individual grains, small domain size retained, as indicated in XRD pattern. On the other hand, the bulk particles formed using the direct sol-gel synthesis at 1000 ºC.

Figure 5 summarizes the size and phase properties of the catalysts made by the PEFP method and sol-gel synthesis at different temperatures. For sol-gel synthesis, pyrochlore phase formed when temperature raised to about 1000 ºC. Amorphous mixture of precursors was found when temperature was around 600 ºC. For the PEFP synthesis, however, pyrochlore phase could form at 550 ºC. RuO_2 together with amorphous mixtures were found at 500 ºC. When the low-temperature made $Y_2Ru_2O_{7-\delta}$ pyrochlore (PEFP-550) was further annealed at 1000 ºC, the particles sintered and resulted in an average grain size of about 200 nm. This result shows the advantage of PEFP synthesis, which effectively reduces the formation temperature of pyrochlore phase and minimizes the sintering of nanoparticles.

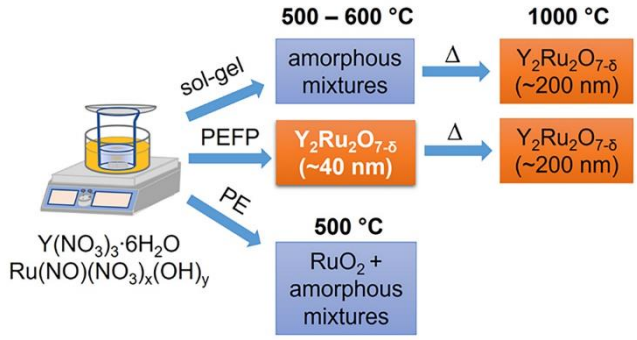

Fig. 5 Schematic of the synthesis of yttrium ruthenate OER electrocatalysts by PEFP and sol-gel methods under different synthesis conditions.

Electrochemical testing of OER performance for nanoscale yttrium ruthenate electrocatalyst

Cyclic voltammogram (CV), Tafel plot, and chronopotentiometry tests were carried out to characterize the OER performance of these $Y_2Ru_2O_{7-\delta}$ electrocatalysts (PEFP-550) and compared with those of reference catalysts (solgel-1000 and IrO_2). **Figure 6a** shows the CV curves of the two $Y_2Ru_2O_{7-\delta}$ electrocatalyst samples. The onset potential of PEFP-550 was measured to be 1.42 V versus RHE and the current density was 6.19 mA/cm^2 at 1.50 V. The solgel-1000 sample exhibited an onset potential of 1.42 V, which is the same as that of PEFP-550, but a lowered current density of 3.61 mA/cm^2 at 1.50 V. In comparison, both RuO_2 and IrO_2 reference catalysts exhibited onset potentials about 1.47 V. The current density was 0.97 mA/cm^2 at 1.50 V for RuO_2 and 0.56 mA/cm^2 at 1.55 V for IrO_2.[8, 10]

Figure 6b shows the Tafel plots to further examine the OER kinetics of those two catalysts. The Tafel slope of PEFP-550 $Y_2Ru_2O_{7-\delta}$ electrocatalyst was calculated to be ~37 mV/dec, while the Tafel slope of solgel-1000 was measured to be ~41 mV/dec. These results suggest that the associated OER kinetics of PEFP-550 catalyst should be similar to that of the solgel-1000. Tafel slopes for both catalysts are lower than that of RuO_2 (60 mV/dec) and IrO_2 (49 mV/dec), indicating better electrocatalytic performance of the pyrochlore catalyst.[9, 10] However, PEFP-550 possessed a better OER activity than the solgel-1000, primarily due to small particle size and relatively high surface area. The difference in current density between the two became larger at high overpotential (η), thus PEFP-550 electrocatalyst had an even better performance at the potential above 1.6 V.

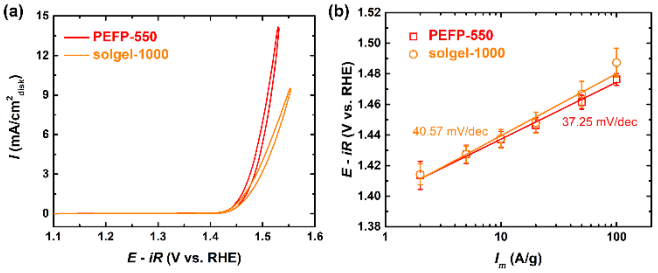

Fig. 6 (a) CV curves and (b) Tafel plots of the PEFP-550 and solgel-1000 OER catalysts in 0.1 M $HClO_4$.

Chronopotentiometry test was performed to examine the OER durability. To facilitate the electrical conductivity of the electrode, 0.75 mg of PEFP-550 was loaded onto a 1 cm × 1 cm carbon paper. **Figure 7a** shows the comparative catalyst stability tested in the chronopotentiometry measurement at a constant current density of 10 mA/cm^2 for 20 h. Oxidation of carbon was negligible as the carbon paper showed no significant current in the CV tests with applied potential. The results indicate the overpotential for PEFP-550 was about 0.27 V and remained constant during the entire testing period. In comparison, the commercial IrO_2 OER catalyst had an overpotential of 0.59 V which was more than double that of the PEFP-550. TEM study shows crystalline structures were observed from surface to bulk with no amorphous surface layer after the OER durability test (**Figure 7b**). The lattice fringes were calculated to be 0.29 nm which is corresponding to the (222) plane of the cubic phase $Y_2Ru_2O_{7-\delta}$.

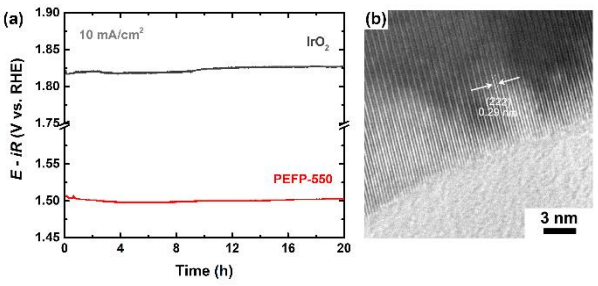

Fig. 7 (a) Chronopotentiometry of the PEFP-550 OER catalyst in 0.1 M $HClO_4$ and (b) representative TEM micrograph of this catalyst after the OER durability test. Chronopotentiometry was performed at a constant current density of 10 mA/cm^2 for 20 h. IrO_2 catalyst was included for comparison.

Electrochemical impedance spectroscopy (EIS) analysis was performed to characterize the properties of these electrocatalysts under different potentials. **Figure 8** shows the Nyquist plots for PEFP-550 and solgel-1000 electrocatalysts measured under no applied potential, at 1.42 V (onset), and 1.50 V, respectively. The equivalent electrical circuit is consisting of solution resistance (R_s), charge transfer resistance (R_{ct}) and double layer capacitance (C_{dl}). The charge transfer resistance is used to examine the catalytic charge transfer rate and estimated using the semi-circle diameters in the Nyquist plot.[8, 44] When no potential was applied, the charge transfer resistances were reflected to the intrinsic conductivity of the OER catalyst (**Figure 8a**).[8, 45] The data shows that the PEFP-550 electrode had a better conductivity than the solgel-1000. With smaller size, PEFP-550 catalyst nanoparticles distributed more evenly in the conducting carbon support than the solgel-1000, thus had a better overall conductivity. When potentials were applied and oxygen evolution started, the PEFP-550 electrode exhibited much smaller charge transfer resistance than the solgel-1000, indicating that PEFP-550 electrode had a faster OER rate (**Figure 8b** and **8c**).

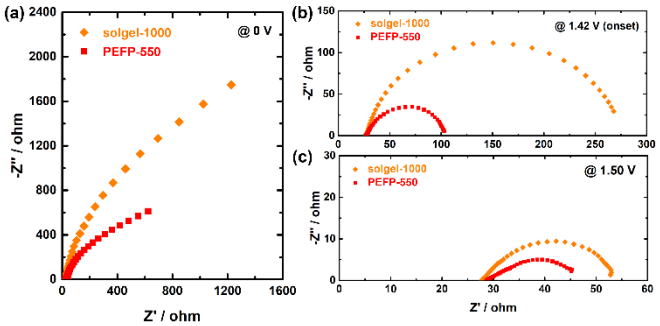

Fig. 8 EIS analysis of PEFP-550 and solgel-1000 OER catalysts at applied potentials of (a) 0 V, (b) 1.42 V (onset), and (c) 1.50 V, respectively.

X-ray absorption spectroscopy (XAS) analysis on the catalyst structures

We characterized the structures of the PEFP-550 OER catalysts using XAS analysis and Ru foil and RuO_2 as the references. XANES of Ru K-edge shows the absorption edge energy (E_0) is 22129.9 eV for the PEFP-550 electrocatalyst and 22125.7 eV for Ru reference and 22132.3 eV for RuO_2 (**Figure 9a**).[36] The oxidation state of Ru in the PEFP-550 was calculated by a linear fit of absorption edge energy and valence states of known Ru references, where Ru foil is zero and RuO_2 is 4.[8, 46] **Figure 9a** inset shows the relationship between edge energy and Ru oxidation state. The oxidation sate of Ru was determined to

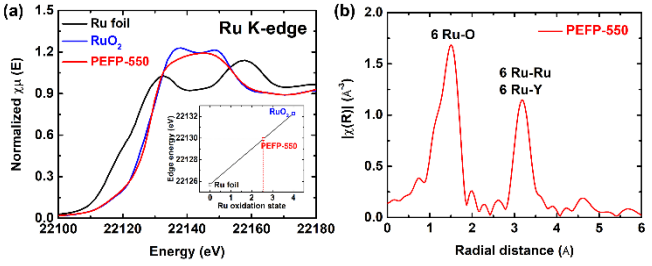

Fig. 9 (a) XANES and (b) Fourier transformed EXAFS spectra of the PEFP-550 OER catalyst. RuO_2 powder and Ru foil were used as the references. Inset in (a) shows the relationship between Ru K-edge energy and oxidation state of the specimens.

be +2.6 for the PEFP-550 catalyst. This result suggests the PEFP-550 catalyst has a high concentration of oxygen defects, which is beneficial to the high OER activity.[4, 9] This large number of oxygen defects may result from the incomplete condensation in this low-temperature synthesis of pyrochlore-type $Y_2Ru_2O_{7-\delta}$.

EXAFS analysis was performed to study the local Ru-O bonding structures and configurations of neighboring atoms. **Figure 9b** shows the k^2-weighted Fourier Transform (FT) radial structure spectra of Ru K-edge for PEFP-550 catalyst. The peak at around 1.5 Å in radial distance is associated to the electron back scattering and corresponds to the first shell Ru-O_6. The bond distance of Ru-O was analyzed by simulating the $Y_2Ru_2O_7$ pyrochlore structure in 1 – 2 Å radial distance.[47] The Ru-O bonding distance for the PEFP-550 was determined as 1.99 Å, which also agrees with the value for $Y_2Ru_2O_{7-\delta}$ catalyst previously reported.[8]

Conclusions

In summary, we successfully developed the PEFP method to produce phase-pure 40 ± 10 nm $Y_2Ru_2O_{7-\delta}$ pyrochlore at a low temperature of 550 ºC. This nm-sized $Y_2Ru_2O_{7-\delta}$ pyrochlore exhibited an overpotential of 270 mV towards the OER at a current density of 10 mA/cm^2 in 0.1 M perchloric acid electrolyte. The high activity and stability of this low-temperature produced $Y_2Ru_2O_{7-\delta}$ pyrochlore can be attributed to nm-sized particles distributed well in conductive support, allowing for the electrocatalytic reaction to operate under low overpotential conditions in acid. This work provides a design strategy for synthesizing phase-pure Ir-free ternary oxide electrocatalysts, which are active and stable for catalyzing the OER in acid under ultralow overpotential conditions.

Experimental Section

Synthetic Procedures

PEFP method was developed to prepare phase-pure pyrochlore $Y_2Ru_2O_{7-\delta}$ with small particle size. In a typical procedure, 20 wt.% of polyvinyl alcohol (PVA, Mw = 9,000 ~ 10,000, Sigma-Aldrich) solution was prepared by dissolving 0.01196 g of PVA in 10 mL of de-ionized water (DIW, 18.2 MΩ-cm) in a 50-mL beaker and stirred for overnight. Stoichiometric amounts of 0.1915 g of yttrium nitrate ($Y(NO_3)_3{\cdot}6H_2O$, 99.9%, Alfa Aesar) and 3.087 mL of ruthenium nitrosyl nitrate ($Ru(NO)(NO_3)_x(OH)_y$ where x+y =3, Sigma-Aldrich) were dissolved in 10 mL of DIW in a 50-mL beaker and stirred for 5 min, followed by addition of the above PVA solution and 1 mL of nitric acid (70 %). This mixture was stirred for another 1 h and then the beaker was transferred to an oil bath at 70 ºC and heated for 5 h. This reaction vessel was then set aside at ambient room conditions overnight to allow water to evaporate, followed by vacuum evaporation at 80 ºC for 6 h. A gel was formed and placed on a hot plate (VWR 7×7″ CER Hot/Stir 120 V Pro) at 300 ºC for 2 h. Colour of the solid changed from brownish to dark grey, while the gel turned into solid after this process. The powder was then collected and placed in a combustion boat, flash pyrolyzed at 550 ºC for 6 h in a pre-heated tube furnace (Thermo Scientific Lindberg/Blue M) to form the final products.

For study of effect of PVA to metal ions ratio on the structure of final product, the amounts of Y and Ru precursors were fixed. Corresponding amount of PVA was calculated and prepared at 20 wt.% for the synthesis. To study the effect of synthetic temperature, we kept all procedures the same except the final annealing step. For those without using the flash pyrolysis, ramping rate was 5 ºC/min without pre-heating furnace. The furnace was pre-heated to the desired temperature at a rate of 50 ºC/min. Once the temperature was stabilized, the combustion boat inside a quartz tube was placed inside the furnace immediately to reduce the temperature fluctuation. After the heating, all samples were cooled down to room temperature naturally.

Characterizations

The crystal phases were analysed by XRD (Rigaku Miniflex 600) with Cu X-ray source. The measurement was performed in the scan range between 10° and 80° 2θ. HRTEM images were taken with a JEOL 2100 Cryo TEM at an acceleration voltage of 200 kV. TEM specimen was prepared by dispersing a suspension in ethanol on a carbon-coated copper grid. SEM images were obtained with a Hitachi S4700 SEM at an acceleration voltage of 10 kV. EDS was collected in the same microscope as the SEM at a voltage of 20 kV. SEM specimen was prepared by directly depositing powder samples on carbon tape on a SEM stub. The average diameter of the particles was calculated based on the SEM image.

Nitrogen isotherm and Brunnauer-Emmett-Teller (BET) analysis was performed using Micromeritics Gemini VII 2390 and 3Flex Physisorption system. The BET surface area of the catalysts was obtained with six-point measurement in the P/P_0 range between 0.05 and 0.30 under an N_2 adsorption environment.

X-ray absorption spectroscopy (XAS) was performed in transmission mode at Beamline 20-BM-B at the Advanced Photon Source (APS), Argonne National Laboratory, USA. The obtained XAS spectra was analyzed by Artemis and Athena software. The RuO_2 powder (99.9%, Sigma-Aldrich) was used as the reference.

Electrocatalytic Property Study

In a typical procedure to make catalyst ink for electrode, 0.5 mL of 0.1 M NaOH solution was added to 0.5 mL of Nafion 117 aqueous solution (5%, Sigma-Aldrich) to obtain a neutralized Nafion solution, of which the pH value was about 8. 2 mg of pyrochlore oxide catalyst, 2 mg of carbon black (Vulcan XC-72), and 3 µL of neutralized Nafion solution were added in 2 mL of tetrahydrofuran (THF) in a 15-mL vial, followed by sonication for 30 min in an ice bath. A glassy carbon rotating disk electrode (RDE) was polished with 0.05 µm alumina slurry until a mirror surface was obtained. 5 µL of the prepared ink solution was drop-casted on the RDE. After the ink dried, 10 µL of Nafion-THF solution (3 µL of neutralized Nafion solution in 2 mL of THF) was drop-casted on top of the disk surface to form a thin film electrode.

Electrocatalytic characterizations were performed using a three-electrode system with a CHI 760D potentiostat (CH Instruments, Inc.). A platinum wire (diameter: 0.5 mm) connected with platinum foil (area: 1 cm^2) was used as the counter electrode, and a hydrogen reference electrode (HydroFlex, Gaskatel) was used as the reference electrode. The reference electrode was calibrated in H_2-saturated (Airgas Inc., 99.999%) 0.1 M $HClO_4$ (Veritas double distilled, 70%) electrolyte solution, where cyclic voltammetry (CV) scans were carried out at a scan rate of 100 mV s^{-1} for 100 s and the average value of the two potentials at which the H_2 oxidation/evolution curves crossed at zero current was treated as the thermodynamic potential for the reversible hydrogen electrode (RHE). In a typical half-cell study, a RDE, platinum wire and hydrogen reference electrode were used as working, counter and reference electrodes, respectively.

OER measurements were performed three times after purging with O_2 (Airgas Inc., 99.999%) for at least 30 min. CV curves were collected at a scan rate of 10 mV s^{-1} in a potential range between 1.1 and 1.6 V versus RHE. The RDE rotating speed was set at 1,600 rpm. All measurements were performed in O_2-saturated 0.1 M perchloric acid solution. The

resistance of the system was measured to be 24-29 Ω, and these values were used for correcting the ohmic resistance. The capacitance was corrected by taking the average value of anodic and cathodic scans to evaluate the electrochemical performance. A commercially available IrO_2 powder (99%, Alfa Aesar) was used as the reference electrocatalyst. Carbon paper (Sigracet 29 BC, Fuel Cell Store) was used as the substrate for the chronopotentiometry tests. The dimension of the carbon paper is 1 cm wide and 3 cm long, with a working area of 1 cm × 1 cm.

Acknowledgements

This work was supported by the University of Illinois. The EM characterizations were carried out at the Frederick Seitz Materials Research Laboratory Central Facilities. The X-ray diffraction was carried out at the George L. Clark X-Ray Facility and 3M Materials Laboratory, School of Chemical Science at UIUC. This research used resources of the Advanced Photon Source at Argonne National Laboratory and was supported by the U.S. DOE under Contract No. DE-AC02-06CH11357 and the Canadian Light Source and its funding partners. We thank Ms. Lei Pan for carrying out preliminary experiments.

Keywords: pyrochlore • yttrium ruthenate • nanocrystalline • oxygen evolution electrocatalyst • polymer entrapment

[1] C. Spöri, J. T. H. Kwan, A. Bonakdarpour, D. P. Wilkinson, P. Strasser, *Angewandte Chemie International Edition* **2017**, *56*, 5994-6021.

[2] J. Suntivich, K. J. May, H. A. Gasteiger, J. B. Goodenough, Y. Shao-Horn, *Science* **2011**, *334*, 3.

[3] Z. W. Seh, J. Kibsgaard, C. F. Dickens, I. Chorkendorff, J. K. Nørskov, T. F. Jaramillo, *Science* **2017**, *355*.

[4] J. T. Mefford, X. Rong, A. M. Abakumov, W. G. Hardin, S. Dai, A. M. Kolpak, K. P. Johnston, K. J. Stevenson, *Nature Communications* **2016**, *7*, 11053.

[5] H.-S. Oh, H. N. Nong, T. Reier, A. Bergmann, M. Gliech, J. Ferreira de Araújo, E. Willinger, R. Schlögl, D. Teschner, P. Strasser, *Journal of the American Chemical Society* **2016**, *138*, 12552-12563.

[6] J. Hwang, R. R. Rao, L. Giordano, Y. Katayama, Y. Yu, Y. Shao-Horn, *Science* **2017**, *358*, 751-756.

[7] N. Danilovic, R. Subbaraman, K. C. Chang, S. H. Chang, Y. Kang, J. Snyder, A. P. Paulikas, D. Strmcnik, Y. T. Kim, D. Myers, V. R. Stamenkovic, N. M. Markovic, *Angewandte Chemie International Edition* **2014**, *53*, 14016-14021.

[8] J. Kim, P.-C. Shih, K.-C. Tsao, Y.-T. Pan, X. Yin, C.-J. Sun, H. Yang, *Journal of the American Chemical Society* **2017**, *139*, 12076-12083.

[9] J. Kim, P.-C. Shih, Y. Qin, Z. Al-Bardan, C.-J. Sun, H. Yang, *Angewandte Chemie International Edition* **2018**, *57*, 13877-13881.

[10] P.-C. Shih, J. Kim, C.-J. Sun, H. Yang, *ACS Applied Energy Materials* **2018**, *1*, 3992-3998.

[11] E. Fabbri, T. J. Schmidt, *Acs Catal* **2018**, *8*, 9765-9774.

[12] H. Jin, C. Guo, X. Liu, J. Liu, A. Vasileff, Y. Jiao, Y. Zheng, S.-Z. Qiao, *Chemical Reviews* **2018**, *118*, 6337-6408.

[13] A. Jain, Y. Shin, K. A. Persson, *Nature Reviews Materials* **2016**, *1*, 15004.

[14] R. Wu, B. Xiao, Q. Gao, Y.-R. Zheng, X.-S. Zheng, J.-F. Zhu, M.-R. Gao, S.-H. Yu, *Angewandte Chemie* **2018**, *130*, 15671-15675.

[15] H. Li, S. Chen, Y. Zhang, Q. Zhang, X. Jia, Q. Zhang, L. Gu, X. Sun, L. Song, X. Wang, *Nature Communications* **2018**, *9*, 2452.

[16] L. Yu, J. F. Yang, B. Y. Guan, Y. Lu, X. W. Lou, *Angewandte Chemie International Edition* **2018**, *57*, 172-176.

[17] J. S. Yoo, X. Rong, Y. Liu, A. M. Kolpak, *Acs Catal* **2018**, *8*, 4628-4636.

[18] C. Lei, H. Chen, J. Cao, J. Yang, M. Qiu, Y. Xia, C. Yuan, B. Yang, Z. Li, X. Zhang, L. Lei, J. Abbott, Y. Zhong, X. Xia, G. Wu, Q. He, Y. Hou, *Advanced Energy Materials* **2018**, *8*, 1801912.

[19] H. B. Tao, Y. Xu, X. Huang, J. Chen, L. Pei, J. Zhang, J. G. Chen, B. Liu, *Joule* **2019**, *3*, 1-12.

[20] G. S. Hutchings, Y. Zhang, J. Li, B. T. Yonemoto, X. Zhou, K. Zhu, F. Jiao, *Journal of the American Chemical Society* **2015**, *137*, 4223-4229.

[21] J. Yu, Q. J. He, G. M. Yang, W. Zhou, Z. P. Shao, M. Ni, *Acs Catal* **2019**, *9*, 9973-10011.

[22] W. G. Hardin, D. A. Slanac, X. Wang, S. Dai, K. P. Johnston, K. J. Stevenson, *The Journal of Physical Chemistry Letters* **2013**, *4*, 6.

[23] C. C. L. McCrory, S. Jung, I. M. Ferrer, S. M. Chatman, J. C. Peters, T. F. Jaramillo, *Journal of the American Chemical Society* **2015**, *137*, 4347-4357.

[24] H. N. Nong, H.-S. Oh, T. Reier, E. Willinger, M.-G. Willinger, V. Petkov, D. Teschner, P. Strasser, *Angewandte Chemie International Edition* **2015**, *54*, 2975-2979.

[25] Y. Lee, J. Suntivich, K. J. May, E. E. Perry, Y. Shao-Horn, *Journal of Physical Chemistry Letters* **2012**, *3*, 399-404.

[26] N. Danilovic, R. Subbaraman, K.-C. Chang, S. H. Chang, Y. J. Kang, J. Snyder, A. P. Paulikas, D. Strmcnik, Y.-T. Kim, D. Myers, V. R. Stamenkovic, N. M. Markovic, *The Journal of Physical Chemistry Letters* **2014**, *5*, 2474-2478.

[27] S. H. Oh, R. Black, E. Pomerantseva, J.-H. Lee, L. F. Nazar, *Nature Chemistry* **2012**, *4*, 1004-1010.

[28] O. Diaz-Morales, S. Raaijman, R. Kortlever, P. J. Kooyman, T. Wezendonk, J. Gascon, W. T. Fu, M. T. M. Koper, *Nature Communications* **2016**, *7*, 12363.

[29] K. Sardar, S. C. Ball, J. D. B. Sharman, D. Thompsett, J. M. Fisher, R. A. P. Smith, P. K. Biswas, M. R. Lees, R. J. Kashtiban, J. Sloan, R. I. Walton, *Chemistry of Materials* **2012**, *24*, 4192-4200.

[30] W. Sun, J.-Y. Liu, X.-Q. Gong, W.-Q. Zaman, L.-M. Cao, J. Yang, *Scientific Reports* **2016**, *6*, 38429.

[31] L. C. Seitz, C. F. Dickens, K. Nishio, Y. Hikita, J. Montoya, A. Doyle, C. Kirk, A. Vojvodic, H. Y. Hwang, J. K. Norskov, T. F. Jaramillo, *Science* **2016**, *353*, 1011-1014.

[32] D. Lebedev, M. Povia, K. Waltar, P. M. Abdala, I. E. Castelli, E. Fabbri, M. V. Blanco, A. Fedorov, C. Copéret, N. Marzari, T. J. Schmidt, *Chemistry of Materials* **2017**, *29*, 5182-5191.

[33] L. Yang, G. Yu, X. Ai, W. Yan, H. Duan, W. Chen, X. Li, T. Wang, C. Zhang, X. Huang, J.-S. Chen, X. Zou, *Nature Communications* **2018**, *9*, 5236.

[34] J. B. Goodenough, R. Manoharan, M. Paranthaman, *Journal of the American Chemical Society* **1990**, *112*, 2076-2082.

[35] J. Parrondo, M. George, C. Capuano, K. E. Ayers, V. Ramani, *Journal of Materials Chemistry A* **2015**, *3*, 10819-10828.

[36] J. Park, M. Park, G. Nam, M. G. Kim, J. Cho, *Nano Letters* **2017**, *17*, 3974-3981.

[37] K. Sardar, E. Petrucco, C. I. Hiley, J. D. B. Sharman, P. P. Wells, A. E. Russell, R. J. Kashtiban, J. Sloan, R. I. Walton,

Angewandte Chemie International Edition **2014**, *53*, 10960-10964.
[38] C. Zener, *Physical Review* **1951**, *82*, 403-405.
[39] J. Kim, X. Chen, Y.-T. Pan, P.-C. Shih, H. Yang, *Journal of The Electrochemical Society* **2017**, *164*, F1074-F1080.
[40] M. H. Nguyen, S.-J. Lee, W. M. Kriven, *Journal of Materials Research* **2011**, *14*, 3417-3426.
[41] D. Ribero, W. M. Kriven, *Journal of Materials Research* **2015**, *30*, 2133-2143.
[42] G. Xiong, S. Yu, X. Yang, L. Lu, X. Wang, *Gongneng Cailiao/Journal of Functional Materials* **1998**, *29*, 92-95.
[43] A. A. Ismail, *Applied Catalysis B: Environmental* **2005**, *58*, 115-121.
[44] T. Audichon, T. W. Napporn, C. Canaff, C. Morais, C. Comminges, K. B. Kokoh, *The Journal of Physical Chemistry C* **2016**, *120*, 2562-2573.
[45] C.-C. Hu, K.-H. Chang, M.-C. Lin, Y.-T. Wu, *Nano Letters* **2006**, *6*, 2690-2695.
[46] S. Riegg, A. Reller, A. Loidl, S. G. Ebbinghaus, *Dalton Transactions* **2015**, *44*, 10852-10859.
[47] Y.-Y. Hu, Z. Liu, K.-W. Nam, O. J. Borkiewicz, J. Cheng, X. Hua, M. T. Dunstan, X. Yu, K. M. Wiaderek, L.-S. Du, K. W. Chapman, P. J. Chupas, X.-Q. Yang, C. P. Grey, *Nature Materials* **2013**, *12*, 1130.

Entry for the Table of Contents

FULL PAPER

Polymer entrapment flash pyrolysis method was developed to prepare nanoscale, iridium-free oxygen evolution electrocatalyst exhibiting an overpotential of 270 mV at 10 mA/cm^2 in perchloric acid solution.

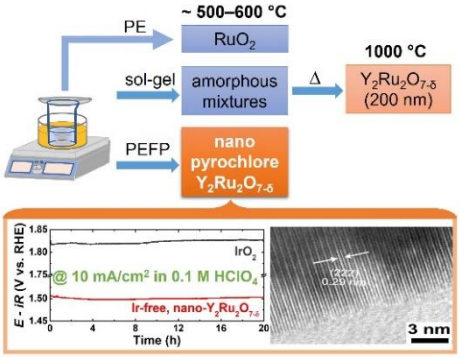

*Pei-Chieh Shih, Cheng Zhang, Harshit Raheja, Cheng-Jun Sun, Hong Yang**

Page No. – Page No.

Polymer Entrapment Flash Pyrolysis for the Preparation of Nanoscale Iridium-Free Oxygen Evolution Electrocatalysts

Additional Author information for the electronic version of the article.

Hong Yang: 0000-0003-3459-4516